Design of Broadband Infrared Photodetectors Enhanced by Dual-Mode Plasmonic Resonant Cavities

Jiayuan Du
Fudan University
Xinyu Zhao
Fudan University
Xiaodong Sun
Fudan University
Jinyao Zeng
Fudan University
Xinhua Hu (huxh@fudan.edu.cn)
Fudan University https://orcid.org/0000-0003-3153-7612

Research Article

Keywords: plasmonic, mercury cadmium telluride (MCT)

Posted Date: August 2nd, 2021

DOI: https://doi.org/10.21203/rs.3.rs-720463/v1

Version of Record: A version of this preprint was published at Plasmonics on October 12th, 2021. See the published version at https://doi.org/10.1007/s11468-021-01552-0.

Design of broadband infrared photodetectors enhanced by dual-mode plasmonic resonant cavities

Jiayuan Du,[1] Xinyu Zhao,[1] Xiaodong Sun,[1] Jinyao Zeng,[1] and Xinhua Hu[1,2]

[1] *Department of Materials Science and Key Laboratory of Micro- and Nano-Photonic Structures (Ministry of Education), Fudan University, Shanghai 200433, China*

[2] *Corresponding author: huxh@fudan.edu.cn*

(Dated: July 18, 2021)

Abstract

The signal-to-noise ratio of infrared photodetectors can be improved by using resonant cavities, whereas the enhancement effect usually occurs in a narrow wavelength range. Here, we propose a dual-mode plasmonic resonant cavity which can enhance the performance of infrared photodetectors in a wide range of wavelengths from 3.5 μm to 5.5 μm. The optical cavity consists of an Au grating, an ultrathin (310 nm) detective layer of mercury cadmium telluride, and an Au film, which can exhibit nearly perfect absorption at resonant wavelengths with using optimal parameters. For the target wavelength range, the wavelength-averaged absorption in the detective layer can also be 62%, about 12 times of that without the resonant cavity. Such a high enhancement of absorption can occur for incident light in a broad range of angle ($\theta < 45^0$) and with different polarizations.

INTRODUCTION

Infrared photodetectors and imaging systems are important in applications including night vision, environmental monitoring, and astronomy research [1]. A significant issue for infrared photodetectors is noise caused by thermal fluctuation that will disturb the detection of signals [2–4]. To suppress the noise, a small volume of detective material can be adopted in photodetectors [2–4], whereas it will reduce the absorbed light power. To enhance light absorption, optical resonant cavities can be further applied [5–21]. However, high absorption enhancement has usually been demonstrated for infrared photodectection in a narrow wavelength range.

Recently, metasurfaces have been constructed to realize high light absorption in a broad band, where multiple distinct metallic resonators exist in a unit cell [22–24]. Such metasurfaces enable strong thermal emission, whereas they cannot be directly applied to enhance infrared photodetection. To enhance infrared photodetection, detective materials need to be incorporated in the structures and infrared light in target wavelength ranges should be absorbed mainly by detective materials rather than metal. In addition, it would be better to adopt connected metallic patterns in the metasurfaces which can serve as electronic contacts. However, such requirements have not been met in previous designs.

In this paper, we propose a plasmonic resonant cavity which can enhance the performance of infrared photodetectors in a broad range of wavelengths from 3.5 μm to 5.5 μm. The optical cavity consists of an Au grating, an ultrathin (310 nm) detective layer of mercury cadmium telluride (MCT) [4], and an Au film, where the metal regions also serve as electric contacts. We show that by using appropriate structural parameters, two optical resonant modes can exist simultaneously in the target wavelength range, and the whole structure can exhibit nearly perfect absorption at resonant wavelengths. The wavelength-averaged absorption in the detective layer over the target wavelength range can be 62%, about 12 times of that without using the resonant cavity.

RESULTS

The photonic structure under study is an MCT layer with thickness t, which is in the x-y plane and sandwiched between an Au grating and an Au film, as shown in Fig. 1a and

b. The top Au grating is an Au film perforated by a square lattice of square holes with size Δ and period a. Both the top Au grating and bottom Au film possess the same thickness t_0. The structure is illuminated by light propagating in the x-z plane that has an incident angle θ and wavelength λ. A finite-element method is adopted to simulate the light absorption in the structure based on COMSOL MULTIPHYSICS commercial software. Here, the permittivity of gold is described by the Lorentz-Drude model [25], and the permittivity of MCT ($Hg_{0.83}Cd_{0.17}Te$) is about $13 + i0.87$ in the target wavelength range (from 3.5 μm to 5.5 μm) [26].

We first consider a photonic structure with parameters of $a = 2.4$ μm, $\Delta = 0.85a$, $t = 0.31$ μm, $t_0 = 0.1$ μm. Figure 2a shows the absorption spectrum at normal incidence, where two absorption peaks can be observed. The whole structure exhibits nearly perfect absorption at resonant wavelengths of $\lambda_1 = 4.29$ μm and $\lambda_2 = 5.11$ μm. The absorption in the MCT layer is about 80% at the resonant wavelengths, which is about 16 times of that in a free-standing MCT layer [Fig. 2b]. For the target wavelength range, the MCT layer can also possess a high wavelength-averaged absorption (62%), much higher than that in a free-standing MCT layer (5%). Such a high absorption enhancement remains for a wide range of incident angles ($\theta < 45^0$) and for different polarizations [Fig. 2c and d].

The distribution of electromagnetic power loss density q in the MCT layer is also calculated at resonant wavelengths, as shown in Fig. 1c. At resonant wavelength of $\lambda_1 = 4.29$ μm, the maximal absorption occurs in the MCT region beneath the hole [Fig. 1c]. However, the MCT region under the metal strongly absorbs light at resonant wavelength of $\lambda_2 = 5.11$ μm [Fig. 1c]. We note that if the top Au grating is removed, the absorption will be uniform in the MCT layer. In addition, the field decay along the z direction is different for the two resonant modes [Fig. 1d]. For the mode with the longer resonant wavelength, the field decays more quickly in the z direction and is more localized in the x-y plane.

The above simulations indicate that the resonant cavity possesses two resonant modes, which can substantially increase the absorption in the MCT layer. To understand the origin of the two resonant modes, we simulate the absorption for an MCT layer with thickness t in three different structures at normal incidence, as shown in Fig. 3. For a free-standing MCT layer, maximal absorption can occur at resonant wavelength

$$\lambda_{R1} = 2nt/m, \tag{1}$$

where n is the real part of the refractive index of MCT and m is a positive integer [Fig. 3a]. When the MCT film is coated on an Au film [Fig. 3b], maximal absorption exists at lower resonant wavelengths

$$\lambda_{R2} = 4nt/(2m-1). \tag{2}$$

Such a resonant mode can split into two modes when an Au grating is covered on the MCT-Au bilayer structure, as shown in Fig. 3c. For the fundamental mode with $m = 1$, the mode splitting occurs in a wide range of thickness ($0.2\ \mu\text{m} < t < 0.5\ \mu\text{m}$). As will be shown, the occurrence of the mode splitting strongly depends on the parameters of the Au grating including the hole size Δ and period a. If the hole size or the period is much smaller than the working wavelength ($\Delta < 0.3\lambda_{R2}$ or $a < 0.3\lambda_{R2}$), the Au grating will behaves like a uniform film so that the fundamental resonant mode will not split. This also explains why the mode splitting effect has not been discovered in previous studies [7]. In fact, when the period is much smaller than the working wavelength, the top Au grating will provide the same reflection phase as the bottom Au film, and thus the resonant wavelength of the Au grating-MCT-Au sandwiched structure will be given by Eq. (1).

Figure 3d shows the wavelength-averaged absorption in the MCT layer over the target wavelength range for the three structures. Since two absorption peaks simultaneously occur in the target wavelength range, the Au grating-MCT-Au sandwiched structure enables higher wavelength-averaged absorption in the MCT layer than the other two structures. When the thickness $t = t_{opt} = 0.31\ \mu\text{m}$, the MCT layer in the sandwiched structure can possess a maximal average absorption in the target wavelength range. Such an optimal thickness can also be estimated by

$$t_{opt} = \lambda_c/(4n) \tag{3}$$

where $\lambda_c = 4.5\ \mu\text{m}$ is the central wavelength of the target spectral range.

The two absorption peaks in Fig. 2 originates from the splitting of the fundamental resonant mode with $m = 1$ in the MCT-Au bilayer structure. To learn more about the mode splitting effect, we simulate the sandwiched structures with different hole size Δ in the Au grating, as shown in Fig. 4a. Here, the parameters are $a = 2.4\ \mu\text{m}$, $t = 0.31\ \mu\text{m}$, and $t_0 = 0.1\ \mu\text{m}$. When $\Delta = a$, a single resonant mode occurs at wavelength of $\lambda_{R2} = 4.5\ \mu\text{m}$. When the hole size of grating Δ is appropriately chosen ($0.76 < \Delta/a < 0.9$), the resonant

mode will split into two modes at wavelengths of λ_1 and λ_2

$$\lambda_i \approx \lambda_{R2} + \beta_i(0.9 - \Delta/a) \tag{4}$$

where $\lambda_{R2} = 4nt$, and $\beta_1 = -1.44$ μm and $\beta_2 = 9.33$ μm for $a = 2.4$ μm. The difference between the two resonant wavelengths increase with decreasing the hole size. Compared with the larger resonant wavelength λ_2, the smaller resonant wavelength λ_1 is closer to the original resonant wavelength λ_{R2}. The wavelength-averaged absorption $\langle A \rangle$ in the MCT layer over the target wavelength range strongly depends on the hole size. When $\Delta/a = 0.85$, the average absorption $\langle A \rangle$ in the MCT layer can reach maximum (62%), as shown in Fig. 4b. When $\Delta/a < 0.3$, the sandwiched structure will not enhance the absorption in the MCT layer.

We also investigate the influence of the grating period a on the absorption in the MCT layer in the sandwiched structure, as shown in Fig. 4c. Here, the parameters are $\Delta/a = 0.85$, $t = 0.31$ μm, and $t_0 = 0.1$ μm. When $a < 0.35\lambda_c$, a single resonant mode exist in the target wavelength range and the wavelength-averaged absorption in the MCT layer increases with increasing the period a, as shown in Fig. 4d. However, when $a > 0.35\lambda_c$, two resonant modes occur in the target wavelength range, resulting in a high wavelength-averaged absorption in the MCT layer (from 54% to 64%). Here, the smallest optimal period can be estimated by

$$a_{opt} \approx \lambda_c/2 \tag{5}$$

When the optimal period is adopted, the wavelength-averaged absorption in the MCT layer over the target wavelength range can reach a local maximum (62%).

CONCULSION

In summary, we have investigated the enhancement effect of a plasmonic resonant cavity on MCT infrared photodetectors working in the wavelength range from 3.5 μm to 5.5 μm. The resonant cavity is composed of an Au grating, an MCT layer, and an Au film, which can support two resonant modes in the target wavelength range. By optimizing the structural parameters, the whole structure can exhibit perfect absorption at resonant wavelengths. The wavelength-averaged absorption in the MCT layer over the target wavelength range can be 62%, about 12 times of that without the resonant cavity. Such a high enhancement

of absorption can occur for incident light in a broad range of angle ($\theta < 45^0$) and with different polarizations.

Author Contributions X. H. and J. D. concieved and designed the study. J. D. performed the simulations. J. D. and X. H. presented the theory and prepared the manuscript. All authors discussed the results and contributed to the final version of the manuscript.

Funding This work was supported by the National Key Research and Development Program of China (2018YFA0306201) and NSFC (61422504 and 11574037).

Conflicts of interest/Competing interests Not applicable.

Data Availability The datasets generated during and/or analyzed during the current study are available from the corresponding author on reasonable request.

Code availability Not applicable.

DECLARATIONS

Ethics approval Not applicable.

Consent to Participate Informed consent was obtained from all authors.

Consent for Publication The authors confirm that there is informed consent to the publication of the data contained in the article.

Conflicts of Interest The authors declare no competing interests.

References

[1] *Handbook of Infrared Detection Technologies*, edited by Henini M and Razeghi M (Elsevier, Oxford, 2002), p. 6.

[2] Rogalski A, Antoszewski J, Faraone L (2009) Third-generation infrared photodetector arrays. J. Appl. Phys. 105: 091101.

[3] Martyniuk P, Antoszewski J, Martyniuk M, Faraone L, Rogalski A (2014) New concepts in infrared photodetector designs. Appl. Phys. Rev. 1: 041102.

[4] Lei W, Antoszewski J, Faraone L (2015) Progress, challenges, and opportunities for HgCdTe infrared materials and detectors. Appl. Phys. Rev. 2: 041303.

[5] Yu Z, Veronis G, Fan S, Brongersma ML (2006) Design of midinfrared photodetectors enhanced by surface plasmons on grating structures. Appl. Phys. Lett. 89: 151116.

[6] Landy NI, Sajuyigbe S, Mock JJ, Smith DR, Padilla WJ (2008) Perfect Metamaterial Absorber. Phys. Rev. Lett. 100: 207402.

[7] Hu X, Li M, Ye Z, Leung WY, Ho KM, Lin SY (2008) Design of midinfrared photodetectors enhanced by resonant cavities with subwavelength metallic gratings. Appl. Phys. Lett. 93: 241108.

[8] Chang CC, Y. D. Sharma YD, Y.-S. Kim YS, J. A. Bur JA, R. V. Shenoi RV, S. Krishna S, D. Huang D, and S.-Y. Lin SY (2010) A surface plasmon enhanced infrared photodetector based on InAs quantum dots. Nano Lett. 10: 1704.

[9] Wu W, Bonakdar A, Mohseni H (2010) Plasmonic enhanced quantum well infrared photodetector with high detectivity. Appl. Phys. Lett. 96: 161107.

[10] Lee SC, Krishna S, Brueck SRJ (2010) Light direction-dependent plasmonic enhancement in quantum dotinfrared photodetectors. Appl. Phys. Lett. 97: 021112.

[11] Zhang C, Chang H, Zhao D, Hu X (2013) Design principle of Au grating couplers for quantum-well infrared photodetectors. Opt. Lett. 38: 4037.

[12] Zhao F, Zhang C, Chang H, Hu X (2014) Design of plasmonic perfect absorbers for quantum-well infrared photodetection. Plasmonics 9: 1397.

[13] Nolde JA, Kim M, Kim CS, Jackson EM, Ellis CT, Abell J, Glembocki OJ, Canedy CL, Tischler JG, Vurgaftman I, Meyer JR, Aifer EH (2015) Resonant quantum efficiency enhance-

ment of midwave infrared nBn photodetectors using one-dimensional plasmonic gratings. Appl. Phys. Lett. 106: 261109.

[14] Lu R, Ge CW, Zou YF, Zheng K, Wang DD, Zhang TF, Luo LB (2016) A localized surface plasmon resonance and light confinement-enhanced near-infrared light photodetector. Laser Photon. Rev. 10: 595–602.

[15] Tang X, Wu GF, Lai KWC (2017) Plasmon resonance enhanced colloidal HgSe quantum dot filterless narrowband photodetectors for mid-wave infrared. J. Mater. Chem. C 5: 362.

[16] Qi Z, Zhai Y, Wen L, Wang Q, Chen Q, Iqbal S, Chen G, Xu J, Tu Y (2017) Au nanoparticle-decorated silicon pyramids for plasmon-enhanced hot electron near-infrared photodetection. Nanotechnology 28: 275202.

[17] Yakimov AI, Kirienko VV, Bloshkin AA, Armbrister VA, Dvurechenskii AV, Hartmann JM (2017). Photovoltaic Ge/SiGe quantum dot mid-infrared photodetector enhanced by surface plasmons. Opt. Express 25: 25602-25611.

[18] Venuthurumilli PK, Ye PD, Xu X (2018) Plasmonic Resonance Enhanced Polarization-Sensitive Photodetection by Black Phosphorus in Near Infrared. ACS Nano 12: 4861.

[19] Tong JC, Suo F, Ma JHZ, Tobing LYM, Qian L, Zhang DH (2019) Surface plasmon enhanced infrared photodetection. Opto-Electron Adv. 2: 180026.

[20] Zhen T, Zhou J, Li Z, Chen X (2019) Realization of both high absorption of active materials and low ohmic loss in plasmonic cavities. Adv. Opt. Mater. 7: 1801627.

[21] Tong JC, Suo F, Tobing LYM, Xu Z, Xiong Y, Zhang DH (2020) Rotated fourfold U-shape metasurface for polarization-insensitive strong enhancement of mid-infrared photodetection. Opt. Express 28: 4225-4233.

[22] Bouchon P, Koechlin C, Pardo F, Haidar R, Pelouard JL (2012) Wideband omnidirectional infrared absorber with a patchwork of plasmonic nanoantennas. Opt. Lett. 37: 1038.

[23] Cheng CW, Abbas MN, Chiu CW, Lai KT, Shih MH, Chang YC, Wide-angle polarization independent infrared broadband absorbers based on metallic multisized disk arrays, Opt. Exp. 20, 10376 (2012).

[24] Zhou L, Tan Y, Ji D, Zhu B, Zhang P, Xu J, Gan Q, Yu Z, J. Zhu J (2016) Self-assembly of highly efficient, broadband plasmonic absorbers for solar steam generation. Sci. Adv. 2: e1501227.

[25] Rakic AD, Djurisic AB, Elazar JM, Majewski ML, Optical properties of metallic films for

vertical-cavity optoelectronic devices, Applied Optics **37**, 5271–5283 (1998).

[26] Chu JH, Li B, Liu K, Tang DY (1994) Empirical rule of intrinsic absorption spectroscopy in $Hg_{1-x}Cd_xTe$, Journal of Applied Physics 75: 1234–1235.

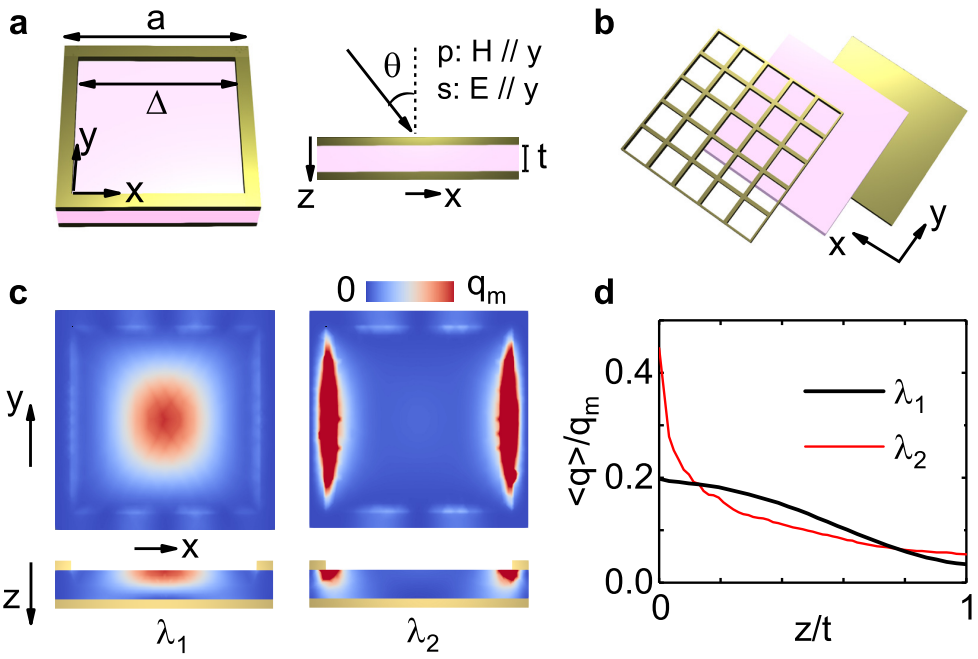

FIG. 1. (Color online) A photonic structure and its resonant modes. The structure consists of an Au grating with thickness t_0, an MCT active layer with thickness t, and an Au film with thickness t_0. The Au grating has a hole size Δ and period a. **a** A unit cell of the structure, which is illuminated by light at incident angle θ. **b** Three layers in the structure. **c** Distribution of electromagnetic power loss density q in the MCT layer at resonant wavelengths of $\lambda_1 = 4.29$ μm and $\lambda_2 = 5.11$ μm. The top panels are at the upper surface of the MCT layer ($z = 0$), while the bottom panels are in the x-z plane and across the center of the hole. Other parameters are the same as in Fig. 2. **d** The average of q in the x-y plane as a function of z.

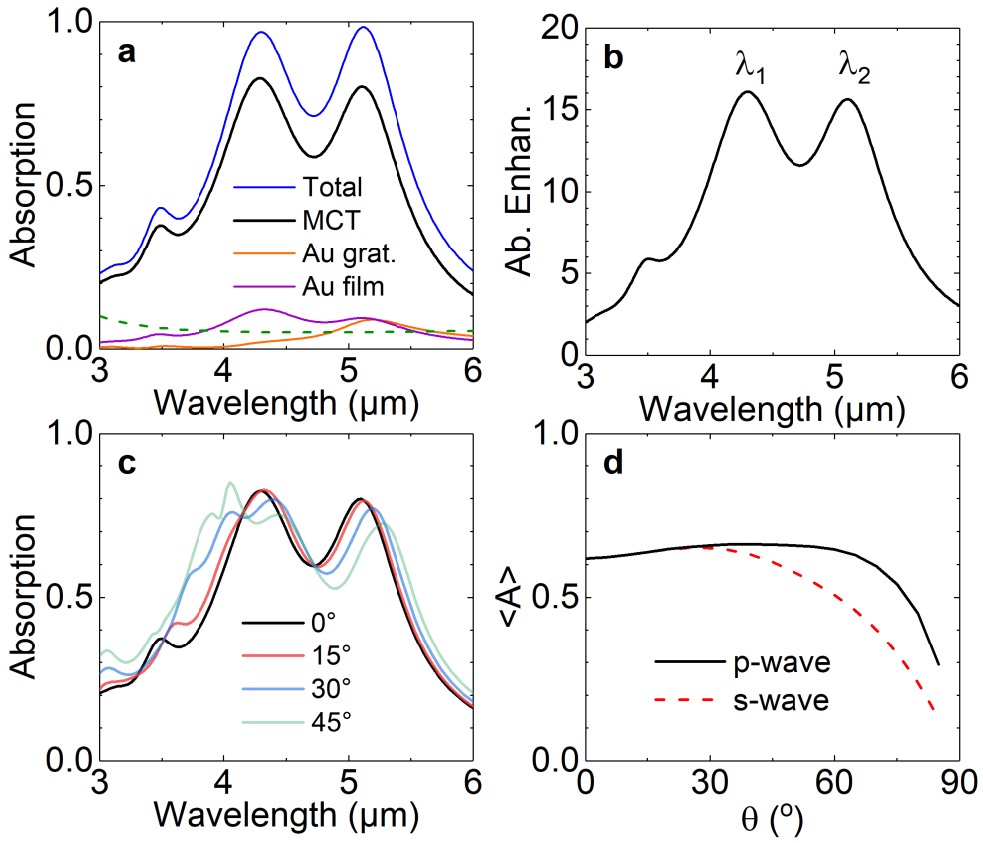

FIG. 2. (Color online) Absorption in the photonic structure in Fig. 1 with parameters of $a = 2.4$ μm, $\Delta = 0.85a$, $t = 0.31$ μm, and $t_0 = 0.1$ μm. **a** Absorption spectra of the whole structure and each layer. The dashed line is the absorption of a free-standing MCT layer with thickness of 0.31 μm. **b** Absorption enhancement of the MCT layer by the photonic structure. **c** Absorption spectra of the MCT layer at different incident angles for p-polarized light. **d** Wavelength-averaged absorption in the MCT layer over the target wavelength range (from 3.5 μm to 5.5 μm) as a function of incident angle.

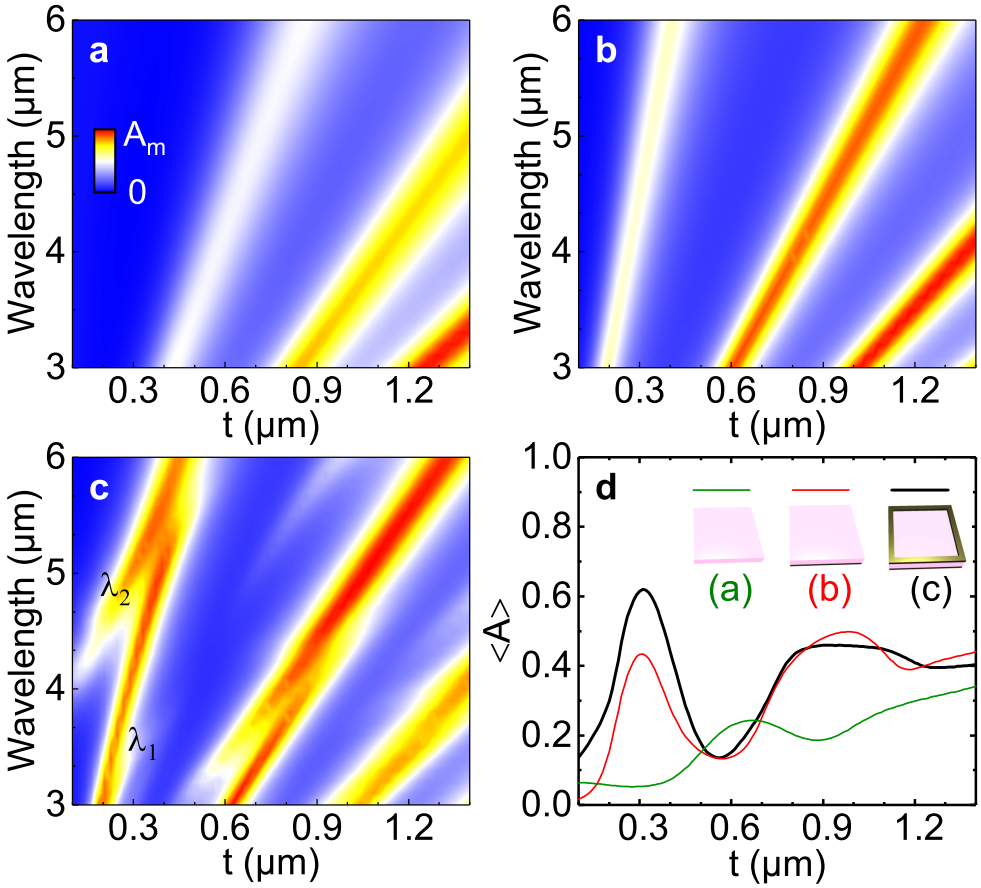

FIG. 3. (Color online) Absorption of an MCT layer with thickness t in three different structures. **a** Absorption of a free-standing MCT layer. **b** Absorption of an MCT layer that is coated on an Au film with thickness of 0.1 μm. **c** Absorption in the MCT layer in the structure in Fig. 1 with $a = 2.4$ μm, $\Delta = 0.85a$, and $t_0 = 0.1$ μm. **d** Wavelength-averaged absorption $\langle A \rangle$ in the MCT layer over the target wavelength range.

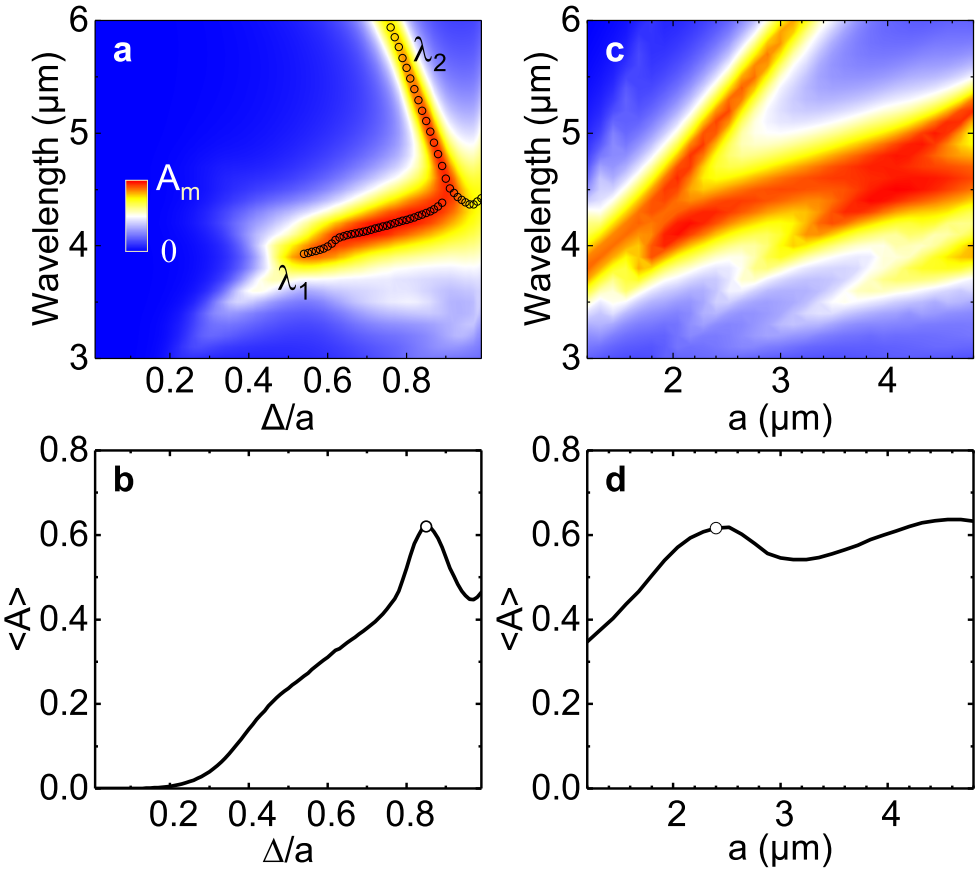

FIG. 4. (Color online) Absorption of the MCT layer in the structure in Fig. 1 with $t = 0.31$ μm and $t_0 = 0.1$ μm. **a** Absorption spectrum and **b** wavelength-averaged absorption $\langle A \rangle$ in the MCT layer over the target wavelength range as a function of hole size Δ with $a = 2.4$ μm. **c** Absorption spectrum and **d** wavelength-averaged absorption $\langle A \rangle$ in the MCT layer as a function of period a with $\Delta = 0.85a$.